

Efficient uncertainty minimization for spectral macrostate data clustering

Brian S. White* and David Shalloway†

Biophysics Program, Department of Molecular Biology and Genetics, Cornell University, Ithaca, New York 14853

Spectral clustering, which uses the global information embedded in eigenvectors of an inter-item relationship matrix, can outperform traditional approaches such as k -means and hierarchical clustering. Spectral hierarchical bipartitioning is well-understood, but spectral multipartitioning remains an interesting research topic. Korenblum and Shalloway [Phys. Rev. E **67**, 056704 (2003)] used an analogy to the dynamic coarse-graining of a stochastic system and the principle of cluster uncertainty minimization to motivate a fuzzy spectral multipartitioning method, macrostate data clustering (MDC), that could solve problems that defeated other methods. However, MDC poses a challenging non-convex global optimization problem that was solved by a brute-force technique unlikely to scale to problem sizes beyond $O(10^2)$. Here we provide further tests of the accuracy of MDC and develop a new method for solving the optimization problem, which can handle data sets at least two orders of magnitude larger. This range includes problems of significant biological interest such as microarray analysis of gene expression data. In addition, we show how clustering by uncertainty minimization is related to and generalizes clustering motivated by perturbative analysis of almost-block-diagonal matrices.

I. INTRODUCTION

Coarse-graining data items i ($1 \leq i \leq N$) into clusters α ($1 \leq \alpha \leq m$) is important for large-scale data analysis. For example, clustering genes according to their microarray expression profiles allows biologists to subsequently infer potential *cis*-regulatory elements from sequence commonalities within the clusters [1]. A clustering solution defines *assignment vectors* $\mathbf{w}_\alpha \equiv [w_\alpha(1), w_\alpha(2), \dots, w_\alpha(N)]$, where $w_\alpha(i)$ is the “grade of membership” of item i with respect to cluster α . This may be made more precise by insisting on a *fuzzy clustering* solution that satisfies the probabilistic constraints

$$w_\alpha(i) \geq 0 \quad (\forall \alpha, i) \quad (1a)$$

$$\sum_\alpha w_\alpha(i) = 1 \quad (\forall i), \quad (1b)$$

and thus defines $w_\alpha(i)$ as the probability that item i is a member of cluster α . This can be useful in data modeling: The probabilistic assignments of individuals to populations (i.e., clusters) based on genotypic data may indicate the presence of an admixed individual, whose genetic makeup is consistent with several populations, or a migrant, whose relatively weak population assignment may suggest immigration into that population in the distant past [2, 3]. In some cases it is adequate to ignore uncertainty and simply partition the items via a *hard clustering* that enforces $w_\alpha(i) \in \{0, 1\}$. This can be done by quantizing a fuzzy clustering (i.e., assigning item i completely to the cluster having the largest assignment value). Some methods (e.g., k -means) only provide hard clusterings, so no probabilistic information is available.

Clustering typically proceeds from an $N \times N$ *similarity matrix* S , where the off-diagonal element S_{ij} provides an inverse indicator of the “distance” between items i and j . The primary data (e.g., the alignment scores from sequence comparisons or edge weights of a graph) may directly define the S_{ij} . Alternatively, the data may consist of N_D *properties* for each item that can be embedded in a metric space. In that case, the data are consolidated into an $N \times N_D$ matrix X , where X_{ia} is the a^{th} property of item i . For example, in microarray analysis each gene is an item and its properties are its N_D expression levels under N_D different conditions. Distances d_{ij} may be defined via a problem-specific Euclidean metric tensor g :

$$d_{ij} = \left[\sum_{a,b=1}^{N_D} (X_{ia} - X_{ja}) g_{ab} (X_{ib} - X_{jb}) \right]^{1/2}. \quad (2)$$

g is the identity when the properties are independent and need no pre-conditioning (i.e., have equal importance), but may otherwise be adjusted to account for correlations and/or data scale anisotropies. S is then defined by $S_{ij} = f(d_{ij})$, where $S_{ij} \geq 0$ and f is often an exponentially decaying function.

Traditional partitioning methods impose characteristic shapes on the clusters. For example, k -means and complete-linkage clustering generate convex clusters while single-linkage clustering generates unbalanced and straggly clusters [4]. These shapes may not reflect the true geometries of the problem (e.g., the irregular boundaries of an object within an image [5]). However, arbitrary cluster shapes can be generated by *spectral clustering* methods, which have outperformed k -means across several synthetic benchmarks [6, 7, 8]. They accomplish this by analyzing the eigensystem of a *transition* (or *Laplacian* [9]) *matrix* Γ ,

$$\Gamma = D_S - S,$$

where D_S is the diagonal matrix of column sums of S :

*Electronic address: bsw27@cornell.edu

†Electronic address: dis2@cornell.edu

$(D_S)_{jj} = \sum_i S_{ij}$. Hence,

$$\Gamma_{ij} \leq 0 \quad (\forall i \neq j) \quad (3a)$$

$$\mathbf{1} \cdot \Gamma = 0, \quad (3b)$$

where $\mathbf{1}$ is the item-space vector having all components equal to unity and \cdot denotes the normalized item-space inner product: $\mathbf{x} \cdot \mathbf{y} \equiv N^{-1} \sum_{i=1}^N x_i y_i$. These equations imply that the eigenvalues γ_n and left eigenvectors ψ_n of Γ satisfy [10]

$$\gamma_0 = 0; \gamma_{n>0} \geq 0 \quad (4a)$$

$$\psi_0 = \mathbf{1}. \quad (4b)$$

Spectral clustering methods embed each item i into the linear space \mathbb{R}^N using the vector components $\psi_0(i), \psi_1(i), \dots, \psi_{N-1}(i)$ as coordinates. Because the low-frequency eigenvectors have longer “wavelengths,” they provide a natural basis for coarse-graining. Therefore, it is sensible to project into the *low-frequency* (or *clustering*) *subspace* wherein items are represented by the low-frequency *clustering eigenvectors* $\vec{\psi}(i) \equiv [\psi_0(i), \psi_1(i) \dots \psi_{m-1}(i)]$, where m is the number of clusters [11]. While some methods fix m *a priori*, others use a *spectral gap* condition:

$$0 = \gamma_0 < \gamma_1 < \dots \gamma_{m-1} \ll \gamma_m. \quad (5)$$

The presence of such a gap suggests the existence of a corresponding gap in the spatial fluctuation scale (owing to the inverse relationship between frequency and wavelength) that naturally sets a scale for clustering.

Methods differ in how they use the $\vec{\psi}(i)$ to define a clustering. *Spectral bipartitioning* approaches (Ref. [12], for history and review) fix $m = 2$. They order the items according to $\psi_1(i)$ (since ψ_0 is constant and provides no information) and then partition them into hard clusters by choosing a separation point [e.g., according to the sign of $\psi_1(i)$ or its position relative to the median]. These approaches can be extended to $m = 2^k$ clusters by recursion [13], typically after fixing k *a priori*.

Unfortunately, hierarchical bipartitioning sometimes fails to respect natural cluster boundaries, and better results can be obtained using non-hierarchical m -way spectral clustering approaches [14, 15, 16]. One way to do this is to partition the items based on their low-frequency subspace coordinates using k -means [7, 17, 18] or *normalized-cut* objective function minimization [19]. The induced partitionings are necessarily hard.

Korenblum and Shalloway [8] developed a fuzzy m -way spectral clustering method using a different approach: They likened clustering to coarse-graining of a dynamic classical stochastic system [20]. In this picture, each cluster is viewed as a metastable macroscopic state of a diffusive relaxation process governed by Γ , which now acts as a dynamical transition matrix. Their *macrostate data clustering* (MDC) approach defines the \mathbf{w}_α as linear com-

binations of the m clustering eigenvectors,

$$\mathbf{w}_\alpha = \sum_{n=0}^{m-1} M_{\alpha n} \psi_n \equiv \vec{M}_\alpha \circ \vec{\psi}, \quad (6)$$

where the $\vec{M}_\alpha \equiv [M_{\alpha 0}, M_{\alpha 1}, \dots, M_{\alpha(m-1)}]$ are m -vectors, $\vec{\psi} \equiv [\psi_0, \psi_1, \dots, \psi_{m-1}]$, and \circ denotes the inner product over the low-frequency subspace, i.e.,

$$\vec{x} \circ \vec{y} = \sum_{n=0}^{m-1} x_n y_n.$$

Eqs. (1) and the independence of the ψ_n imply constraints on the \vec{M}_α :

$$w_\alpha(i) = \vec{M}_\alpha \circ \vec{\psi}(i) \geq 0 \quad (\forall \alpha, i) \quad (7a)$$

$$\sum_\alpha \vec{M}_\alpha = \hat{\varepsilon}_0, \quad (7b)$$

where $\hat{\varepsilon}_0$ is the m -vector $(1, 0, \dots, 0)$.

Eq. (6) transforms the clustering problem to that of determining the optimal \vec{M}_α subject to Eqs. (7). Since the \mathbf{w}_α are non-negative and composed of only the long-wavelength $\psi_{n < m}$, they will, in general, overlap each other,

$$\mathbf{w}_\alpha \cdot \mathbf{w}_\beta \geq 0, \quad (8)$$

and the item-to-cluster assignments will inherently be uncertain, i.e., fuzzy. In MDC the best clustering is defined as that having *minimum uncertainty*, so the optimal \vec{M}_α , and hence optimal clustering, is determined by minimizing an uncertainty-measuring objective function subject to the constraints of Eqs. (1) [equivalently, Eqs. (7)]. Acceptable clusterings are determined by the spectral gap condition of Eq. (5) and a minimum certainty parameter.

However, uncertainty minimization presents a challenging constrained, non-convex optimization problem. While Korenblum and Shalloway demonstrated the ability of MDC to solve difficult problems, they did so using a “brute-force” solver whose $O(m^2 N^{m+1})$ computational complexity limited its application to modest-sized problems ($N = 200$) and precluded application to the larger problems [e.g., $N \sim O(10^4)$] that emerge in areas such as gene microarray analysis [21].

Weber et al. [22, 23] introduced an efficient approximate fuzzy clustering method that was motivated by perturbative analysis of almost-block-diagonal matrices [24]. Their Perron Cluster Cluster Analysis (PCCA) also uses Eq. (6) but with the \mathbf{w}_α defined as “membership functions” that only approximate the probabilistic non-negativity constraints of Eq. (1a). In PCCA the \vec{M}_α are determined algorithmically, not by objective function optimization, and clusterings for different values of m are accepted if the resultant approximation is regarded by somewhat subjective criteria to be adequate. While approximate, this method had the advantage of being computationally simpler than MDC.

In this paper we show that the MDC uncertainty minimization problem has geometric interpretations that can be exploited to obtain a zeroth-order solution to the global problem, which can then be locally refined towards an exact solution using standard linear programming methods. The algorithm is computationally efficient and allows MDC to solve an $m = 10, N = 20,000$ problem in about one minute on a commodity processor. Secondly, we show that the PCCA membership functions can be viewed as approximate solutions to the minimum uncertainty condition, thus establishing a connection between uncertainty minimization and block-diagonal matrix perturbation. Using this connection, we extend the previously reported conditions under which the PCCA approximation is applicable.

II. REVIEW OF MDC

Shalloway [20] described how spectral analysis of continuous stochastic dynamics can be used to fuzzily dissect configuration space into macroscopic regions (*macrostates*), which provide a coarse-grained representation for describing metastable dynamic relaxations. Korenblum and Shalloway [8] adapted this approach to data clustering by modeling the set of items as a discrete diffusive system and regarding Γ_{ij} as the stochastic transition rate between items i and j . Using dimensional analysis and considering occlusion of diffusive flow by intervening items, they suggested [25]

$$\Gamma_{ij} = -\frac{e^{-(d_{ij})^2/2\langle d_0^2 \rangle}}{(d_{ij})^2} \quad (i \neq j) \quad (9a)$$

$$\Gamma_{ii} = -\sum_{j \neq i} \Gamma_{ji} \quad (9b)$$

$$\langle d_0^2 \rangle = N^{-1} \sum_{i=1}^N (d_{i<})^2, \quad (9c)$$

where $d_{i<} \equiv \min_{j \neq i} d_{ij}$.

Defining the time-dependent ensemble probability vector $\mathbf{p}(t)$, where $p_i(t)$ is the probability of occupation of item i at time t , they then introduced diffusive dynamics using the master equation

$$\frac{d\mathbf{p}(t)}{dt} = -\Gamma \cdot \mathbf{p}(t). \quad (10)$$

Γ has non-negative eigenvalues [8] and its left and right eigenvectors are equal and orthogonal and may be normalized so that

$$\boldsymbol{\psi}_m \cdot \boldsymbol{\psi}_n = \delta_{mn}.$$

Eq. (10) has the solution

$$\mathbf{p}(t) = \sum_{n=0}^{\infty} c_n e^{-\gamma_n t} \boldsymbol{\psi}_n,$$

which describes relaxation to equilibrium. It can be shown that Eqs. (3) and (10) ensure that all components of $\mathbf{p}(t)$ remain non-negative during this relaxation.

This and related [17, 26, 27, 28, 29] dynamical metaphors provide *post facto* justification for common practices within the spectral clustering community, including the form of Γ , the use of low-frequency subspaces, and the requirement for a spectral gap. For example, early approaches [7, 30] analyzed, without explanation, a Γ matrix having an exponential numerator as in Eq. (9a). Moreover, Eq. (3b) [equivalently, Eq. (9b)] is now interpreted as dynamical conservation of probability. Furthermore, since the eigenvalues now describe transition rates, the spectral gap of Eq. (5) indicates that dynamics can be separated into fast modes $\boldsymbol{\psi}_{n \geq m}$ that redistribute probability *within* m weakly-communicating subregions (or clusters) and slow modes $\boldsymbol{\psi}_{n < m}$ that redistribute probability *between* clusters.

MDC determines m by the spectral gap condition and then determines the optimal \vec{M}_α by minimizing the cluster overlap uncertainties expressed by Eqs. (8). As discussed in Ref. [8], minimizing these is equivalent to maximizing the $\mathbf{w}_\alpha \cdot \mathbf{w}_\alpha$. Normalizing for cluster size, MDC maximizes the geometric mean of the *fractional cluster certainties* $\bar{\Upsilon}_\alpha(M)$ ($1 \leq \alpha \leq m$),

$$\bar{\Upsilon}_\alpha(M) \equiv \frac{\mathbf{w}_\alpha \cdot \mathbf{w}_\alpha}{\mathbf{1} \cdot \mathbf{w}_\alpha}, \quad (11)$$

where M represents the components of all the \vec{M}_α . The *overall uncertainty function* $\Phi(M)$,

$$\Phi(M) \equiv -\sum_{\alpha} \log \bar{\Upsilon}_\alpha(M), \quad (12)$$

provides the global minimization objective function that determines M . The clustering specified by this solution is accepted only if

1. The spectral gap condition [Eq. (5)] is satisfied for a *minimum gap parameter* ρ_γ

$$\gamma_m / \gamma_{m-1} > \rho_\gamma. \quad (13)$$

2. The \mathbf{w}_α are not excessively fuzzy. Quantitatively, we require that

$$\bar{\Upsilon}_\alpha(M) > \rho_\Upsilon \quad (\forall \alpha), \quad (14)$$

where ρ_Υ is the *minimum certainty parameter*.

Because $\Phi(M)$ is invariant under permutations of the indices associated with the clusters, its global minimum will have an $m!$ -fold permutation degeneracy.

III. COMPUTATIONAL THEORY

Minimization of $\Phi(M)$ subject to the constraints of Eqs. (7) poses a global, non-linear optimization problem

with respect to the m^2 degrees of freedom of M . We first describe two geometric representations of the problem in Sec. III A that illuminate the problem and then show how to solve it in three steps: (1) precondition Γ to improve numerical efficiency, to remove outliers, and to avoid numerical noise that can obfuscate spectral gaps when low-lying eigenvalues are nearly degenerate (Appendix A), (2) find a zeroth-order solution (Sec. III B), and (3) determine the exact solution by iterative refinement using linear programming with a subset of the inequality constraints (Sec. III C).

A. Geometric representation of uncertainty minimization

1. Symmetric M -representation

Each \vec{M}_α may be regarded as the coordinates of a particle α in \mathbb{R}^m with axes labeled $M_0, M_1, \dots, M_{(m-1)}$. Eq. (7a) implies that the same N inequality constraints act on each particle: The inequality constraints associated with item i are identical for each α and thus restrict each \vec{M}_α to the same feasible half-space in \mathbb{R}^m . This half-space is bounded by a hypersurface that passes through the origin and is normal to $\vec{\psi}(i)$. The intersection of these half-spaces determines the feasible region as a convex polyhedral cone in the upper half of \mathbb{R}^m . Only a subset of the inequality constraints will actually bound the feasible region, since their satisfaction will automatically guarantee satisfaction of the other constraints. And, as proved in Appendix B 1, each particle lies on an edge of the polyhedral cone (i.e., is constrained by $m-1$ active inequality constraints) at every local minimizer of $\Phi(M)$.

An example of this *symmetric M -representation* for $m=2$ is shown in Fig. 1(a). In this case, the feasible region is bounded by only two lines corresponding to $\vec{M} \circ \vec{\psi}(i_<) = 0$ and $\vec{M} \circ \vec{\psi}(i_>) = 0$, where $i_<$ and $i_>$ are the minimizer and maximizer of $\psi_1(i)$, respectively. The global minimum of Φ corresponds to the unique (up to the permutation degeneracy) situation where each particle lies on the feasible region boundary while the equality constraints of Eq. (7b) are simultaneously satisfied. In the example shown in the figure, this is when the points lie within the two squares on the boundary. The two ways of associating the particles with the squares corresponds to the 2-fold permutation degeneracy of the solution.

2. Asymmetric M -representation

The m particles in the symmetric M -representation are not independent because of the equality constraints [Eq. (7b)]. We use these in the *asymmetric M -representation* to explicitly eliminate the degrees of freedom of one *slave* particle that, without loss of generality, we take to be

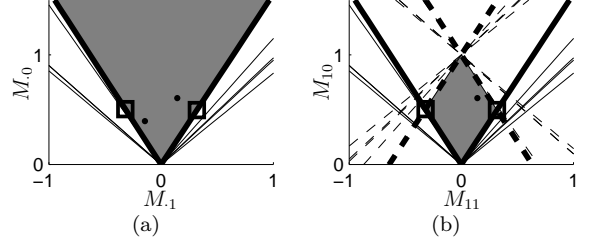


FIG. 1: Symmetric and asymmetric M -representations of an $m=2$ problem. (a) *Symmetric M -representation*: The diagonal lines indicate the boundaries formed by the inequality constraints. The two bold lines forming the narrowest cone (shaded) define the feasible region in $\mathbb{R}^m = \mathbb{R}^2$. \vec{M}_1 and \vec{M}_2 are represented by dots. They are not independent since they are further constrained by the equality constraints of Eq. (7b). The global minimum of the uncertainty objective function $\Phi(M)$ corresponds to the dots being located at the positions indicated by small squares, and the invariance under particle exchange corresponds to the permutation degeneracy discussed in the text. (b) *Asymmetric M -representation*: The solid lines indicate the boundaries of the homogeneous inequality constraints acting on the free particle $\vec{M}^{\text{free}} = \vec{M}_1$. The dashed lines indicate the boundaries of the inhomogeneous inequality constraints that derive from the slave particle \vec{M}_2 . Two of these (bold-dashed) lines cap the cone formed by the relevant homogeneous constraint boundaries (bold) to define a closed feasible polytope in $\mathbb{R}^{m(m-1)} = \mathbb{R}^2$. In this representation the single dot represents all $m(m-1) = 2$ components of \vec{M}^{free} . $\Phi(M)$ is minimized at either of the two permutation-degenerate solutions (small squares).

\vec{M}_m :

$$\vec{M}_m = \hat{\varepsilon}_0 - \sum_{\alpha \neq m} \vec{M}_\alpha. \quad (15)$$

The homogeneous inequality constraints on the slave, $\vec{M}_m \circ \vec{\psi}(i) \geq 0$ ($\forall i$), transform into inhomogeneous inequality constraints that couple the remaining $m-1$ free particles:

$$\sum_{\alpha \neq m} \vec{M}_\alpha \circ \vec{\psi}(i) \leq 1. \quad (16)$$

We consolidate the $m(m-1)$ degrees of freedom of the free particles into the supervector \vec{M}^{free} having components $(\vec{M}_1, \vec{M}_2, \dots, \vec{M}_{m-1})$ in $\mathbb{R}^{m(m-1)}$. Optimization then proceeds in $\mathbb{R}^{m(m-1)}$ with the \vec{M}^{free} restricted by $(m-1)N$ homogeneous inequality constraints from Eq. (7a) with $1 \leq \alpha < m$ and N inhomogeneous inequality constraints from Eq. (16). The combination of homogeneous and inhomogeneous inequality constraints forms a closed convex polytope that bounds the feasible region. Each local minimum of $\Phi(M)$ (and thus, the global minimum) lies at a vertex of this polytope [8].

An example of the asymmetric M -representation for $m=2$ is shown in Fig. 1(b). In this case there are

four bounding constraints: two homogeneous inequality constraints having boundaries passing through the origin and two inhomogeneous inequality constraints (from the slave cluster) with boundaries intersecting at $\hat{\varepsilon}_0$ [31]. Φ is infinite at the polytope vertices at the origin and $\hat{\varepsilon}_0$. The two other vertices correspond to index-permutation-equivalent global minima.

The minimization problem can be visualized and easily solved in this manner only for $m = 2$: As m increases the number of polytope vertices, and hence the number of local minima, grows rapidly, and the global minimization problem becomes difficult. Korenblum and Shalloway [8] used a brute-force method that randomly explored different vertices.

B. Cluster representatives and the approximate global solution

We take a different approach: Rather than trying to identify the global-minimizing vertex directly, we exploit the fact that the m^2 components of M can be determined by the m^2 low-frequency components of an appropriately chosen subset $\mathcal{R} = \{r_1, r_2, \dots, r_m\}$ of m items, which we call *representatives*. To make this explicit we write a matrix analog of Eq. (6) over \mathcal{R} as

$$W^{\mathcal{R}} = M \circ \Psi^{\mathcal{R}}, \quad (17)$$

where

$$\begin{aligned} W_{\alpha\beta}^{\mathcal{R}} &\equiv w_{\alpha}(r_{\beta}) & (1 \leq \alpha, \beta \leq m) \\ \Psi_{n\alpha}^{\mathcal{R}} &\equiv \psi_n(r_{\alpha}) & \begin{cases} (1 \leq \alpha \leq m) \\ (0 \leq n < m) \end{cases} \end{aligned}$$

and M is the matrix having the \vec{M}_{α} as its rows. According to Eq. (7b), M must satisfy

$$\sum_{\alpha} M_{\alpha n} = \delta_{n0}. \quad (19)$$

As shown in Appendix B 2, there always exists at least one subset \mathcal{R} such that $\Psi^{\mathcal{R}}$ is invertible. With such a subset we can solve Eq. (17) for M :

$$M = W^{\mathcal{R}} \bullet (\Psi^{\mathcal{R}})^{-1}, \quad (20)$$

where \bullet denotes the inner product over the cluster index α .

The usefulness of Eq. (20) may be questioned since we do not exactly know any $W^{\mathcal{R}}$ *a priori*. However, any data set amenable to clustering will have at least one item per cluster that will be strongly assigned in the clustering solution; we call such items *candidate representatives*. If we could select a set of representatives \mathcal{R}_c containing one candidate representative from each cluster, we could use our approximate foreknowledge of their assignment values at the solution, $W^{*\mathcal{R}_c}$, to approximate M at the solution, M^* , via Eq. (20).

For example, if item i_{α} were a candidate representative for cluster α , its assignment in the clustering solution would be [32]

$$w_{\beta}^*(i_{\alpha}) \approx \delta_{\alpha\beta}. \quad (21)$$

By choosing $r_{\alpha} = i_{\alpha}$ for cluster α and making similar choices for the other clusters, we would get

$$W^{*\mathcal{R}_c} \approx I.$$

This zeroth-order estimate could be used to approximately solve Eq. (20) for M^* :

$$M^* = W^{*\mathcal{R}_c} \bullet (\Psi^{\mathcal{R}_c})^{-1} \quad (22a)$$

$$\approx I \cdot (\Psi^{\mathcal{R}_c})^{-1} = (\Psi^{\mathcal{R}_c})^{-1} \equiv M^0. \quad (22b)$$

In agreement with Eq. (19), M^0 would satisfy [33]

$$\sum_{\alpha} M_{\alpha n}^0 = \delta_{n0}. \quad (23)$$

Knowing M^0 would allow us to define zeroth-order estimates \mathbf{w}_{α}^0 for *all* the items via Eq. (6) with $\vec{M}_{\alpha} = \vec{M}_{\alpha}^0$, where the \vec{M}_{α}^0 are the rows of M^0 :

$$\mathbf{w}_{\alpha}^0 = \vec{M}_{\alpha}^0 \circ \vec{\psi}. \quad (24)$$

However, the \mathbf{w}_{α}^0 would not necessarily satisfy the inequality constraints of Eq. (1a). If they did, they would solve the optimization problem. If they didn't, they would provide a starting point for refining the solution as discussed in Sec. III C.

1. Finding \mathcal{R}_c

Eq. (22b) implies that we only need to find the representatives to determine M^0 . This is trivial when $m = 2$: The two active inequality constraints [identified by either pair of intersecting bold and bold-dashed lines in Fig. 1(b)] come from the extremal items r_1 and r_2 of ψ_1 , i.e., the minimizer and maximizer of $\psi_1(i)$. Thus, at the solution $w_1^*(r_2) = 0$ and $w_2^*(r_1) = 0$, and the equality constraints imply that $w_1^*(r_1) = 1$ and $w_2^*(r_2) = 1$. Thus, r_1 and r_2 not only generate the active constraints, but are also the representatives, which in this case are perfectly assigned in the solution.

The situation is more complicated when $m > 2$. The representatives: (1) may not be maxima and minima of the eigenvectors, (2) may not be the items associated with the active constraints, and (3) may not be perfectly assigned at the solution. Nonetheless, as discussed above, they will satisfy $w_{\alpha}(r_{\beta}) \approx \delta_{\alpha\beta}$, even for $m > 2$, and we will use this property to identify them.

We show how this is done using the $m = 3$ spiral problem as an example (Fig. 2). In the dataspace [panel (a)] the items form three interlocking crescents in a spiral

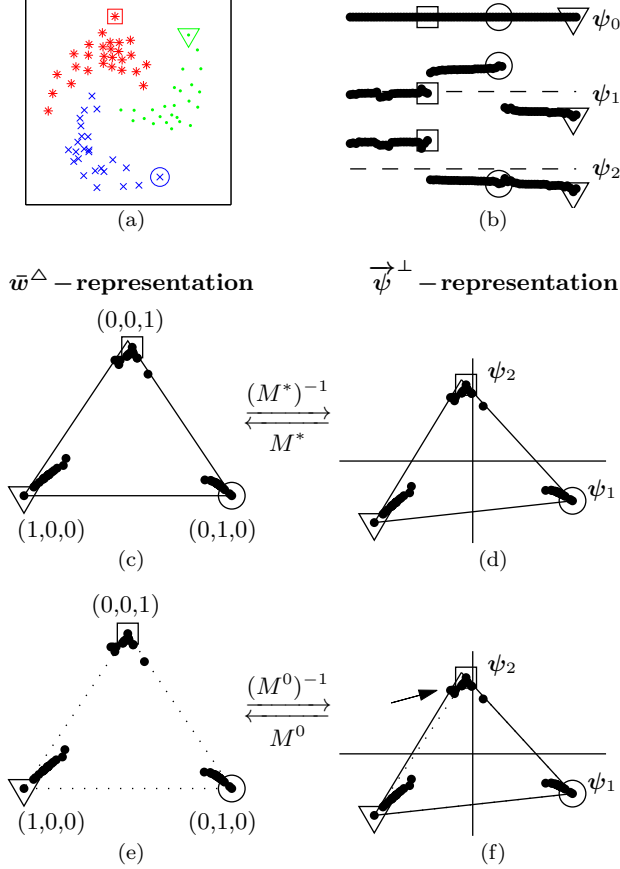


FIG. 2: (Color online) \bar{w}^Δ - and $\vec{\psi}^\perp$ -representations of the spiral problem. The items are represented by points in the 2-dimensional dataspace representation (a), the clustering (low-frequency) eigenvector representation (b), the barycentric coordinates of the \bar{w}^Δ -representation (c) and (e), or the $\vec{\psi}^\perp$ -representation (d) and (f). Panels (c) and (d) correspond to the refined solution M^* , while (e) and (f) correspond to the zeroth-order solution M^0 . The solid and dotted triangles denote the M^* and M^0 feasible region boundaries. [The solid triangle is superimposed in panel (f) to show how the triangle expands slightly in the $\vec{\psi}^\perp$ -representation during refinement. The arrow indicates the item that becomes an active constraint in M^* .] The left and right arrows connecting the representations are reminders that M determines the positions of the items in the \bar{w}^Δ -representation and of the triangle vertices in the $\vec{\psi}^\perp$ -representation. [Although it is not evident in the figure, the points in panels (c) and (e) and the top vertex in panels (d) and (f) are at slightly different positions.] The different item symbols (and colors) used in panel (a) denote the hard clustering obtained by quantizing the MDC fuzzy clustering. The ordering of items in panel (b) was chosen *post facto* to separate the clusters. The dashed lines in this panel are at $\psi_n(i) = 0$. The representatives for clusters 1, 2, or 3 are enclosed within triangles, circles, or squares, respectively.

pattern that makes them difficult to correctly cluster by conventional means. The three low-frequency clustering eigenvectors are shown in panel (b), and the representatives that we would like to find are identified by circles, triangles, and squares. To find \mathcal{R}_c we imagine that we know M^* and the corresponding assignment vectors w_α^* so that we can map this solution into \mathbb{R}^m at the points specified by the 3-vectors $\bar{w}^*(i) \equiv [w_1^*(i), w_2^*(i), w_3^*(i)]$ in panel (c) [34]. Because the $\bar{w}^*(i)$ satisfy the probabilistic equality constraints, these points lie in the 2-dimensional plane that is normal to the vector $(1, 1, 1)$ and at distance $1/\sqrt{3}$ from the origin. Moreover, because they satisfy the probabilistic inequality constraints, the points lie within an equilateral triangle in this plane. (We use “within” to include points that lie on the boundary.) This provides barycentric coordinates [35] in which the three vertices of the triangle correspond to the cluster assignments $(1, 0, 0)$, $(0, 1, 0)$ and $(0, 0, 1)$; we will call these the $\alpha = 1, 2$, and 3 vertices, respectively. The three components of $\bar{w}^*(i)$ are given by the three distances of point i from the three sides of the triangle. Thus, if point i lies on the side of the triangle opposing vertex α , the inequality constraint $w_\alpha(i) \geq 0$ is active. We call this the \bar{w}^Δ -representation [panel (c)]. Although it is not evident in the figure, consistent with the even distribution of active inequality constraints between the clusters (Appendix B 1), each side of the triangle intersects exactly two items.

The candidate representatives are the items that are close to the three vertices, and we want to choose one from the vicinity of each vertex to compose \mathcal{R}_c . We can do this by choosing the three items that (when taken as vertices) define the triangle of largest area. The triangular area defined by a subset \mathcal{R} of any three items located at their solution positions is $|W^{*\mathcal{R}}|/(2\sqrt{3})$. Thus, our task is to identify the \mathcal{R} that maximizes the determinant of $W^{*\mathcal{R}}$.

Since we don’t actually know M^* or the $\bar{w}^*(i)$, it is not obvious how to proceed. However, Eq. (17) implies that

$$|W^{*\mathcal{R}}| = |M^*| |\Psi^{\mathcal{R}}|, \quad (25)$$

so, since M^* is fixed, selecting the \mathcal{R} that maximizes $|W^{*\mathcal{R}}|$ is equivalent to selecting the \mathcal{R} that maximizes $|\Psi^{\mathcal{R}}|$. This is straightforward because $\Psi^{\mathcal{R}}$ does not depend on M . Formally, maximizing $|\Psi^{\mathcal{R}}|$ is a combinatoric problem that could be solved by comparing the determinants for all subsets \mathcal{R} . However, this would be exponentially expensive in N . Instead we use an efficient greedy algorithm that selects the representatives solely from the subset of candidate representatives. This may not exactly maximize the determinant, but will be adequate to determine M^0 .

We leave the details of the greedy algorithm to Appendix C, but it is useful to establish its geometric framework here, while continuing to use the spiral problem as an example: We first plot each item in the 2-dimensional $\vec{\psi}^\perp$ -representation using the 2-vector

$\vec{\psi}^\perp(i) = [\psi_1(i), \psi_2(i)]$ [panels (d) and (f)]. [No information is lost in this projection from the low-frequency subspace since $\psi_0(i) = 1 (\forall i)$.] These vectors are independent of M ; rather, in this representation M determines the position of the inequality constraint bounding triangle [36]. As explained in Appendix B4, the $\vec{\psi}^\perp$ coordinates of the three bounding triangle vertices are the columns of the bottom two rows of M^{-1} . When $M = M^*$ [panel (d)] the vertices may not coincide with any items, but all the items will lie within the bounding triangle. When $M = M^0$ [panel (f)], the triangle vertices coincide with the representatives. In this approximation some items may violate the inequality constraints and lie outside the bounding triangle. (Four items in the upper left corner are outside the triangle in this example.) The greedy algorithm operates within the $\vec{\psi}^\perp$ -representation to identify \mathcal{R}^c .

The approach generalizes easily to higher m : The $\bar{w}^*(i)$ are now m -vectors; the \bar{w}^Δ -representation is in a $(m-1)$ -dimensional hyperplane normal to the vector $(1, 1, \dots, 1)$ in \mathbb{R}^m and provides barycentric coordinates for the $\bar{w}^*(i)$; \mathcal{R}_c is comprised of the subset of m items that, when located at their solution positions in the \bar{w}^Δ -representation, are the vertices of the $(m-1)$ -simplex of largest hypervolume; this hypervolume, for any subset \mathcal{R} , is proportional to $|W^*\mathcal{R}|$ so, via Eq. (25), we can transform the problem of selecting \mathcal{R}_c to that of finding the m items that maximize $|\Psi^\mathcal{R}|$; this problem is equivalent to maximizing the hypervolume of the $\vec{\psi}^\perp$ -representation simplex having vertices at $\vec{\psi}^\perp(i) : i \in \mathcal{R}$. Once \mathcal{R}_c has been identified, it is used to determine M^0 via Eq. (22b), and M^0 is used to determine \mathbf{w}_α^0 via Eq. (24).

C. Refinement

1. Case when M^0 is the exact solution

If the \mathbf{w}_α^0 satisfy all the inequality constraints, they provide the unique solution to the uncertainty minimization problem. To prove this, consider the $\vec{\psi}^\perp$ -representation of an $m = 3$ problem where the inequality constraints are satisfied. As discussed above, transforming M^0 to M moves the sides of the $\vec{\psi}^\perp$ triangle. Moving any side inwards would leave a representative outside the triangle, thus violating an inequality constraint. And, since points are already within the triangle (i.e., all inequality constraints are satisfied), moving any side outwards would result in that side contacting less than two points, i.e., one of the clusters would have less than the required (Appendix B1) $m-1 = 2$ active inequality constraints. Therefore, in this case $M^* = M^0$ must be the unique solution. As can be inferred from the analysis of Fig. 1, M^0 is always the unique solution for $m = 2$ problems.

2. Linearizing $\Phi(M)$

If the \mathbf{w}_α^0 violate any inequality constraints, M^0 is not a solution but can be used as the starting point for further refinement. Since it is expected to be near M^* , we can expand the objective function in its neighborhood as

$$\begin{aligned} \Phi(M) &= -\sum_{\alpha} \log \frac{\vec{M}_{\alpha} \circ \vec{M}_{\alpha}}{\vec{M}_{\alpha} \circ \hat{\varepsilon}_0} \\ &\approx \Phi(M^0) + \sum_{\alpha} \left(\vec{M}_{\alpha} - \vec{M}_{\alpha}^0 \right) \circ \vec{\nabla}_{\alpha} \Phi(M) \Big|_{M=M^0}, \end{aligned} \quad (26)$$

where

$$\vec{\nabla}_{\alpha} \Phi(M) \equiv \frac{\delta \Phi(M)}{\delta \vec{M}_{\alpha}} = -2 \frac{\vec{M}_{\alpha}}{|\vec{M}_{\alpha}|^2} + \frac{\hat{\varepsilon}_0}{\vec{M}_{\alpha} \circ \hat{\varepsilon}_0}$$

is the gradient of $\Phi(M)$ with respect to \vec{M}_{α} . Local minimization using this linear approximation and the constraints of Eqs. (7) poses a linear programming (LP) problem, which can be solved by standard methods.

A simple approach would be to: (1) apply LP, using Eq. (26) and all the constraints, to find an improved, constraint-satisfying solution M^1 , (2) set $M^0 \leftarrow M^1$, and (3) repeat (1) and (2) until sufficient convergence is achieved. This amounts to a constrained variant of gradient-descent local minimization. However, we do not expect to encounter the slow convergence problems that sometimes plague gradient descent because both the LP solution and the true solution are at vertices of the feasible polytope [37]. Therefore, even the first iteration will drive the solution to a vertex, and the solution will not change at the next iteration unless the vertices are very dense on the scale set by the curvature of $\Phi(M)$. Thus, rapid convergence is expected.

3. Reducing the number of constraints included in LP

However, the cost of standard LP solvers (e.g., simplex and interior point methods) grows rapidly [$\mathcal{O}(N_c^{1.5})$] with the number of constraints N_c , which may be large [38]. While there are mN inequality constraints, only $m(m-1)$ of these are active at M^* . These alone need to be included in the LP problem and will guarantee that all the inequality constraints will be satisfied. Since we will often be interested in problems where $m \sim \mathcal{O}(10)$ and $N \sim \mathcal{O}(10^4)$, it would accelerate the LP solver by multiple orders of magnitude if the number of constraints provided to it were reduced to $\sim \mathcal{O}(m)$.

We do not know the active constraints *a priori*, but can find them rapidly by an iterative procedure that exploits the fact that (as discussed above) at M^* exactly $m-1$ points will lie on each of the m faces of the bounding simplex in the $\vec{\psi}^\perp$ -representation. To motivate this procedure, consider the refinement of the spiral problem

(Fig. 2). The left side of the (dotted) M^0 triangle [panel (f)] must move outwards to include the four points in the upper left region that are excluded from its interior; this motion must leave the side intersecting two points. Because the objective function $\Phi(M)$ constitutes an inward “pressure” on the triangle, M^* will correspond to the situation where the smallest expansion that can accomplish this is used. Consequently, the left side will pivot outwards about the lower left corner until it intersects the item identified by the arrow. Each side of the resulting M^* triangle [panel (d)] will intersect $m - 1 = 2$ points, and these points will be near (but not identical with) the $m = 3$ vertices of the M^0 triangle. These six intersections will identify the $m(m - 1) = 6$ active constraints.

This suggests that, for $m = 3$ in general, the two points lying on a side of the M^* triangle will be near different vertices and, subject to this restriction, will be the points that are farthest outside the M^0 triangle. This easily generalizes to $m > 3$: None of the $m - 1$ points that lie on a face of the M^* simplex will be near the same simplex vertex. Of the points near a vertex, it is the ones that are farthest outside the M^0 simplex that are most likely to lie on the M^* simplex. Thus, it is sensible to initially attempt a LP solution using only the inequality constraints corresponding to the $m(m - 1)$ face-item point pairs arising from the $m - 1$ points that are farthest outside each of the m faces. [If point i lies on the face opposing vertex α , this face-item pair corresponds to the active inequality constraint $w_\alpha(i) = 0$.] However, this is only a heuristic argument, and inequality constraints may still be violated in this partially constrained LP solution. If so, we iterate and add to an *included constraint list* \mathcal{C} (of face-item pairs) the violated constraints that are identified by the above criteria as most likely to be active. The procedure terminates when all the inequality constraints are satisfied. Termination is guaranteed because we only add (and never remove) inequality constraints to the included constraint list. The procedure is formalized in the following algorithm:

4. Refinement Algorithm

1. Initialize \mathcal{C} to the empty set.
2. Perform hard clustering based on the M^0 assignments: Item i is assigned to cluster (vertex) α if it is the maximizer of $w_\alpha^0(i)$. We call this subset of items \mathcal{S}_α .
3. For the face opposing vertex α , identify the item i_β from \mathcal{S}_β ($\beta \neq \alpha$) that is farthest outside that face. This identifies the $m - 1$ constraints corresponding to the face-item pairs $(\alpha, i_\beta : \beta \neq \alpha)$. As shown in Appendix B5, the ordering of the item points relative to the simplex faces is the same in the \vec{w}^Δ - and $\vec{\psi}^\perp$ -representations. Therefore, we determine the ordering in the barycentric coordinates of the \vec{w}^Δ -representation since this is simple: $w_\alpha(i)$ is the

distance of an item point i from the α -opposing face (positive if inside, negative if outside the simplex). When executed for the m opposing faces, this procedure identifies $m(m - 1)$ inequality constraints \mathcal{C}' .

4. $\mathcal{C} \leftarrow \mathcal{C} \cup \mathcal{C}'$.
5. Apply the LP solver with the equality constraints, the inequality constraints in \mathcal{C} , and the linear objective function approximation of Eq. (26).
6. Check for satisfaction of all inequality constraints and for convergence according to $\max_{\alpha,i} |\mathbf{w}_\alpha^1(i) - \mathbf{w}_\alpha^0(i)| < \rho_{\text{LP}}$, where ρ_{LP} is a small number, and $\mathbf{w}_\alpha^1(i)$ and $\mathbf{w}_\alpha^0(i)$ are the values determined by M^1 and M^0 , respectively. If both conditions are satisfied, terminate with $M^* = M^1$; if not, set $M^0 \leftarrow M^1$ and return to step 2.

When the algorithm is applied to the spiral problem, \mathcal{C} is set to the active constraints in a single step [39].

D. Recursion

MDC identifies clusters based on the overall size scale of the original dataset. However, once a cluster has been identified and is considered in isolation, the scale will be smaller and subclusters may be apparent. MDC can be reapplied recursively to identify such subclusters.

IV. OVERALL COMPUTATIONAL ALGORITHM

Combining the steps described in Secs. II and III, the overall algorithm is:

1. Compute and precondition Γ as described in Sec. II and Appendix A.
2. Compute 20 low-frequency clustering eigenvalues and eigenvectors [40] using the iterative Lanczos method [41, 42]. This is usually more efficient than computation of the full eigensystem, but it will converge slowly if the eigenvalues are densely-packed near zero (as they often are). To avoid this problem we employ a shift-and-invert spectral transformation [41]

$$(\Gamma - \sigma I)^{-1} \psi_n = \nu_n \psi_n$$

that spreads out the small eigenvalues near σ by transforming them into the large magnitude eigenvalues ν_n of $(\Gamma - \sigma I)^{-1}$,

$$\nu_n = (\gamma_n - \sigma)^{-1}. \quad (27)$$

The eigenvectors are unaffected by the transformation, and the γ_n are easily calculated from Eq. (27).

Since we are interested in the eigenvalues near zero, we choose $\sigma = \sqrt{\epsilon}$, where ϵ is machine precision, to maximize the spread without introducing significant numerical error.

3. Determine m according to the lowest spectral gap satisfying Eq. (13). If there is no gap, the algorithm has determined that there are no clusters and terminates.
4. Identify the representatives and compute the zeroth-order solution M^0 and w_α^0 using the procedure of Sec. III B.
5. Determine whether bfw_α^0 violates any inequality constraints. If so, iteratively refine M^0 to M^* using the procedure of Sec. III C and, via Eq. (6), determine the refined solution w_α^* . Otherwise, $w_\alpha^* = w_\alpha^0$.
6. Test the solution against the minimum certainty conditions of Eq. (14). If it satisfies them, the solution is accepted. If not, the eigenspectrum can be tested for higher spectral gaps, and the algorithm proceeds with step 4. If desired, the fuzzy solution can be quantized to a hard clustering by assigning item each i to the cluster having the largest assignment value.
7. Analyze hard clusters recursively if desired.

V. RESULTS

Korenblum and Shalloway evaluated MDC by solving problems that had challenged traditional clustering methods (e.g., k -means and agglomerative clustering) and by clustering items embedded in a 20-dimensional space to demonstrate that this success was not an artifact of low dataspace dimensionality. To extend these accuracy tests, we considered data sets from the Fundamental Clustering Problems Suite (FCPS) [43]. In addition, to assess the efficiency of the new algorithm, we tested it on synthetic data sets containing up to $N = 20,000$ items.

A. Implementation

The C++ implementation of this algorithm was compiled using `gcc` version 4.1.2 and `g77` version 3.3.5 under `-O3` optimization. The implementation accesses low-level LAPACK [44] routines through LAPACK++ [45] version 2.5.2, interfaces to the ARPACK [46] Lanczos solver through the ARPACK++ C++ wrappers [47], and solves constrained linear programs using the GLPK simplex method [48] version 4.9. The scaling benchmarks of Sec. V C were executed on a dedicated quad CPU 3.46 GHz Pentium 4, configured with 4 GB of RAM and 4 GB of swap space, and running a 64-bit version of SuSE Linux. The numerical precision parameter was

$\epsilon = 2.22045 \times 10^{-16}$. Following Korenblum and Shalloway [8], the dataspace metric tensor g in Eq. (2) was set to the identity, and the minimum gap and minimum certainty parameters were set to $\rho_\gamma = 3$ and $\rho_\Upsilon = 0.68$. The LP convergence parameter was $\rho_{LP} = 0.001$.

B. Performance on FCPS test sets

We tested MDC on the ten FCPS [43] data sets, which were designed to confound traditional methods such as k -means and agglomerative methods. Results for five of these are shown in Fig. 3 and Table I. Results for the others are not shown to conserve space, but reproduce the subjective clusterings suggested by Ultsch [43].

The Lsun [panel (a)] and Target [panel (b)] data sets contain well-separated clusters, which generated nearly disconnected Γ 's. If the preconditioning step (Appendix A) had not been applied, the resulting numerically-degenerate systems would have had multiple near-zero eigenvalues (incorrectly computed because of numerical error) with associated erroneously-mixed eigenvectors. [This is the reason that the ψ_0 eigenvectors displayed in panels (a) and (b) are not constants.] The use of this defective eigensystem was avoided by the connected component analysis of the preconditioning step. This separated the clusters and directly determined the hard assignment vectors shown in the figures.

The Γ matrix of the Two Diamonds data set [panel (c)] was not disconnected, even after preconditioning. The spectral gap separating γ_1 and γ_2 ($\gamma_2/\gamma_1 = 29.3$) properly indicated that there are two clusters. MDC computed the fuzzy assignment vectors shown in the figure. As discussed above, $m = 2$ problems are trivial for MDC, so the M^0 solution was exact and no LP iterations were required. Appropriately, the assignments were very strong (1.00) for items in the middle of the diamonds and weak (~ 0.5) for items near their interface, reflecting the expectation that these items should not be strongly assigned to either cluster. For the most part, the weakly-assigned items are the ones that we have found to be misclassified by single- and complete-linkage methods and k -means (not shown). The overall certainties Υ_α were high (0.93) for both clusters.

The Tetra data set [panel (d)] has four nearly-overlapping tetrahedrally-arranged clusters in a three-dimensional dataspace. MDC correctly determined $m = 4$ from the spectral gap. Since $m > 2$, M^0 was not a feasible solution. The $\sim O(0.01)$ violations of the inequality constraints were refined to M^* by two invocations of the LP solver. As in the case of Two Diamonds, items near the cluster interfaces were given weaker cluster assignments, in this case ranging down to $w_\alpha(i) = 0.74$.

The Engy Time data set [panel (e)] is an overlapping two-dimensional mixture of two Gaussian distributions. The preconditioning step removed a few outliers from the dataset, but because of the strong overlap, MDC assigned all the items to a single cluster. This differed from

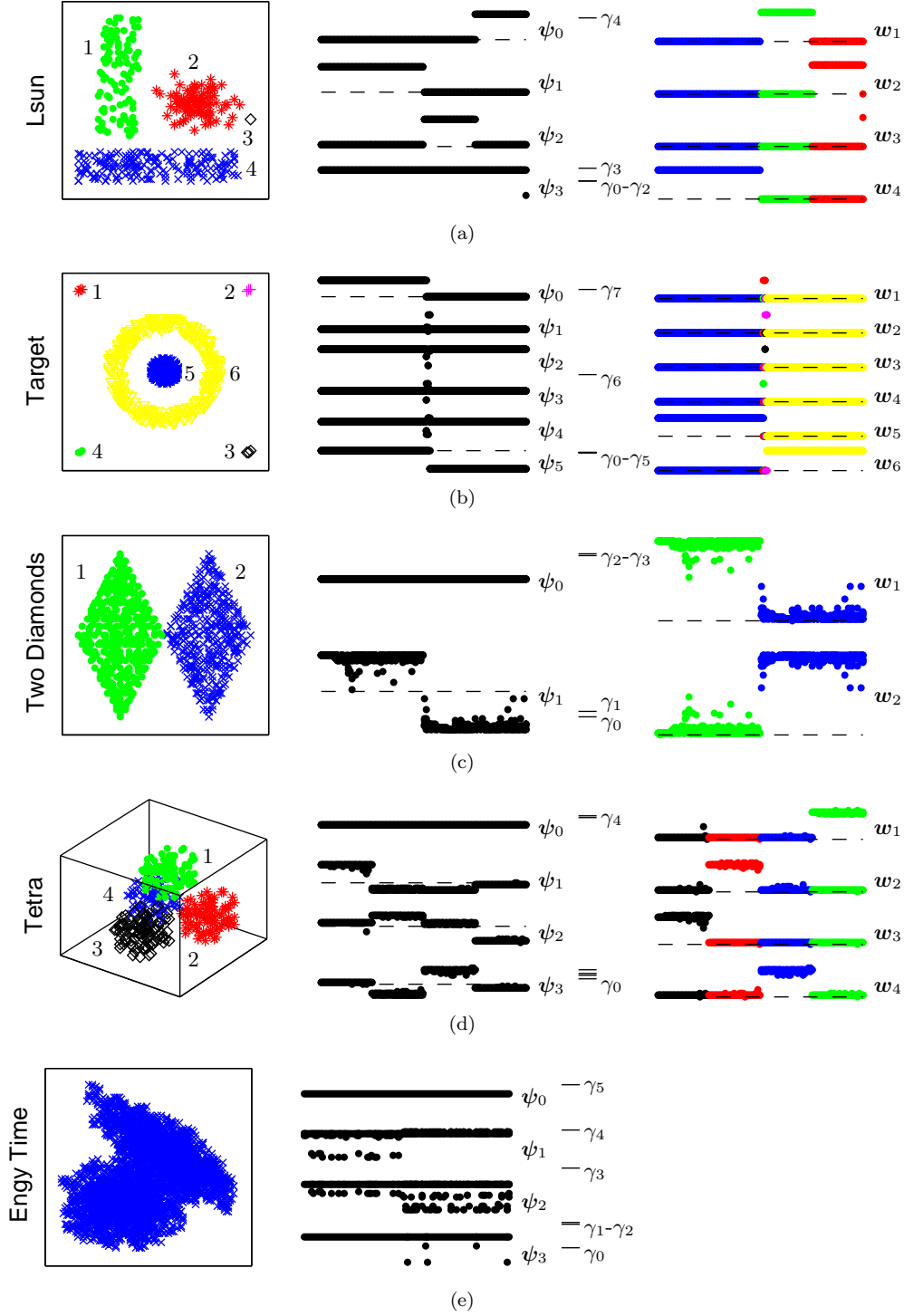


FIG. 3: (Color online) Macrostate data clustering of test cases from the Fundamental Clustering Problems Suite. The data set (left column), eigenvectors ψ_n and eigenvalues γ_n (middle column), and assignment vectors w_α (right column) of the (a) Lsun, (b) Target, (c) Two Diamonds, (d) Tetra, and (e) Engy Time problems are shown. In the left column, the different item symbols (and colors) denote the hard clustering obtained by quantizing the MDC fuzzy clustering. The numbers correspond to the cluster identifiers used in the right column. The ordering of items in the middle and right columns was chosen *post facto* to separate the clusters and would not be evident before the cluster analysis. The points in these panels do not overlap, but only appear to because of limited graphical resolution. The eigenvectors of Lsun and Target are those output by the numerical eigensolver. Because of numerical error they are incorrectly mixed and ψ_0 is not a constant. They are shown for illustration only; as discussed in the text, the solution in this case is determined by the connected component analysis of the preconditioning step.

Ultsch [43], who used a self-organizing map approach incorporating distance and density relations to divide the items into two clusters. We suggest that either choice is acceptable, depending on the application.

Problem	m	$\frac{\gamma_m}{\gamma_{m-1}}$	$\bar{\Upsilon}_\alpha(M)$	Assignments	LP Iterations
Lsun	4	$> \epsilon^{-1/2}$	1.00	Hard Clustering	—
Target	6	$> \epsilon^{-1/2}$	1.00	Hard Clustering	—
Two Diamonds	2	29.30	0.93	0.53–1.00	0
			0.93	0.59–1.00	
Tetra	4	17.20	0.87	0.74–1.00	2
			0.90	0.77–1.00	
			0.91	0.87–1.00	
			0.93	0.55–1.00	
Engy Time	1	—	—	—	—

TABLE I: Quantitative analysis of MDC on bi- and tri-variate Fundamental Clustering Problems Suite test cases. The number of clusters m , the magnitude of the spectral gap γ_m/γ_{m-1} , the cluster certainties $\bar{\Upsilon}_\alpha(M)$, the range of assignment values for each cluster, and the number of iterations of the linear programming solver are listed for each problem. The entry $\gamma_m/\gamma_{m-1} > \epsilon^{-1/2}$, where ϵ is numerical precision, indicates that a clustering was determined by the connected component analysis during the preconditioning phase.

C. Computational efficiency and scaling

To systematically evaluate MDC efficiency and cost scaling with N , we applied it to synthetic data sets containing from 2 to 10 clusters and from 5,000 to 20,000 items arranged in a pyramid of blocks in a two-dimensional dataspace. These problems required from two to four invocations of the LP solver, with the number increasing with m , but not evidently with N . The log-log plot in Fig. 4 shows a clear power-law relation between N and execution time, with time scaling like $O(N^{1.7})$, with little dependence on m . For the largest problems, execution time was dominated by the calculation of Γ and by the eigensolver (each having roughly equal cost), with other contributions totaling less than 4%. The time required for the largest problem ($m = 10$, $N = 20,000$) was only about one minute using a commodity processor. Such problems are of the scale of biological microarray gene expression data sets.

VI. DISCUSSION

Macrostate data clustering (MDC), originally introduced by Korenblum and Shalloway [8], is a fuzzy m -way spectral clustering method motivated by an analogy to the coarse-graining of a physical diffusive system. It uses a heuristic approximation to the physical transition rate

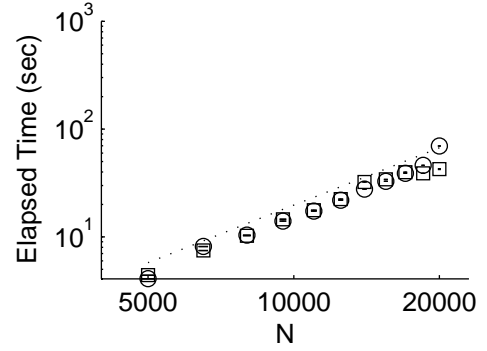


FIG. 4: Log-log plot of elapsed wall-clock time versus N for synthetic benchmarks. N is varied from 5,000 to 20,000 in steps of 1,500. The results shown for $m = 2$ (\circ) and $m = 10$ (\square) are representative of those for intermediate m and are averages over five runs. (The standard errors of the mean are too small to be discernible.) The dotted line is the linear fit and has slope 1.7.

matrix as the Laplacian Γ of spectral clustering. The heart of MDC is its use of the m low-frequency eigenvectors of Γ as a linear basis for expanding (via transformation matrix M) fuzzy cluster assignment vectors \mathbf{w}_α , which probabilistically describe cluster membership. The long-wavelength character of the low-frequency eigenvectors inherently introduces cluster overlap and attendant uncertainty, which leads naturally to an information-theoretic objective function on M that assesses cluster uncertainty. Uncertainty minimization determines the optimal linear relationship, M^* , between the \mathbf{w}_α and the eigenvectors. Spectral gap and minimum uncertainty conditions combine to automatically determine the number of clusters. By exploiting non-linear information preserved in the eigensystem, MDC succeeds on problems where traditional methods such as k -means and agglomerative clustering fail.

Determining the cluster uncertainty minimum poses a challenging non-convex global minimization problem. The solver in the initial implementation of MDC was primarily useful for proof-of-principle: Because of computational inefficiency it was limited to problems with $\sim O(10^2)$ items [8]. To overcome that limitation we developed an efficient global minimization algorithm, which extends the number of items that MDC can rapidly cluster by at least two orders of magnitude; problems with $N \sim O(10^4)$ can be solved within minutes on a commodity processor. We performed additional accuracy tests on MDC and showed that it solves all the problems in the Fundamental Clustering Problems Suite [43], which were designed to challenge traditional clustering methods. We also conducted tests with synthetic data sets ranging in size up to 20,000 items and ten clusters to determine the scaling of computational cost. The dominating computational costs were roughly evenly divided between computation of Γ and of the eigensystem, were insensitive to the number of clusters, and scaled $\sim O(N^{1.7})$. This suggests

that problems containing as many as $N \sim O(10^6)$ items could be solved in reasonable time on a serial machine.

We described the uncertainty minimization problem in four different geometric representations: the m -dimensional symmetric M -representation, the $m(m-1)$ -dimensional asymmetric M -representation, and the $(m-1)$ -dimensional \bar{w}^Δ - and $\vec{\psi}^\perp$ -representations. All are formally equivalent, but each has advantages. The symmetric M -representation has the most direct connection to the minimization problem. The asymmetric M -representation provides a closed (compact) feasible region; it is used to prove that all local minima are at polytope vertices and that the inequality constraints are evenly distributed between the clusters at these points. The \bar{w}^Δ -representation provides barycentric coordinates and elucidates the significance of the m cluster representatives in \mathcal{R}_c as those defining the $(m-1)$ -simplex of largest hypervolume. The $\vec{\psi}^\perp$ -representation motivates the greedy algorithm used to approximate \mathcal{R}_c , which in turn yields an approximation to M^0 , the starting point for refinement to M^* .

The greedy algorithm is the same as the *inner simplex method* used in the Perron Cluster Cluster Analysis method [22, 23] for approximate fuzzy data clustering [49]. However, our motivation for the algorithm, and consequently our understanding of its domain of validity, are different. The inner simplex method was motivated by earlier work [50, 51] on the perturbation theory of block-diagonal matrices [24]. That work exploited two observations: (1) that the Γ of well-separated clusters can be brought into almost-block-diagonal form, and (2) that the low-frequency eigenvectors of such a Γ are perturbed only in second-order in the non-block-diagonal terms, and therefore, to this order, possess a “level structure” in which their eigenvector components concentrate near m different values. The inner simplex method aims at finding one item from each level set and thus, in principle, depends on their existence. In contrast, the analysis presented here makes no assumptions about level structure and only presumes that at least one item (i.e., the representative) can be well-assigned to each cluster. Thus, the approximation is more generally applicable than previously stated. An example where representatives exist even though matrix perturbation theory is no longer applicable and the eigenvectors do not have a level structure is illustrated in Fig. 5(b). Even in this case it is evident that there are three fuzzy clusters, although many of the items will have weak assignments.

In the two-cluster case the M^0 solution is exact, but in all the test problems having more than two clusters, it always violated some of the inequality constraints required for a probabilistic interpretation of the w_α . We remove these violations by using iterative linear programming to minimize the uncertainty objective function subject to the constraints. In the examples tested the corrections were modest, typically changing $w_\alpha(i)$ by $\sim O(0.1)$; in one case (Tetra) they were very small, $\sim O(0.01)$. Thus,

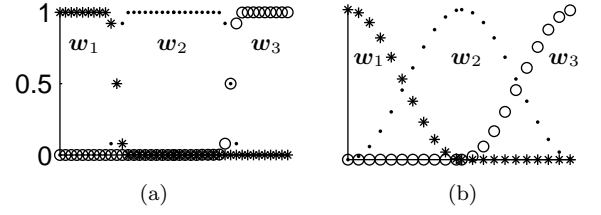


FIG. 5: Assignment vectors for a three-cluster problem for eigenvectors with or without a “level structure.” Eigenvectors arising from almost-block-diagonal Γ have a level structure leading to “almost-hard” assignment vectors such as those shown in panel (a). (Different symbols are used for the three assignment vectors.) When there is no level structure, the assignment vectors are much softer, as in panel (b). However, even in this case representatives (identified by arrows) exist.

except when high accuracy is needed, the main use of the refinement appears to be to provide a rational method for ensuring that the w_α^0 satisfy the probabilistic constraints. Also important is the final value of the the objective function and the fractional cluster certainties $\bar{\Upsilon}_\alpha(M)$. These provide objective measures of the quality of the clusterings, which can be as important to know as the clusterings themselves.

Deuffhard and Weber [52] used a metastability objective function for clustering protein conformations collected from molecular dynamics simulations that is closely related to the sum of the $\bar{\Upsilon}_\alpha(M)$. This is the sum of terms

$$\frac{w_\alpha \cdot e^{-\Gamma t} \cdot w_\alpha}{1 \cdot w_\alpha},$$

where t denotes a time period which, in practice, is set to a multiple of the molecular dynamics integration time step [53, 54]. These terms measure the fractional persistence of probability in macrostate α after stochastic evolution for time t . They are identical to the fractional cluster certainties $\bar{\Upsilon}_\alpha(M)$, defined in Eq. (11), except for the presence of the Markov matrix $e^{-\Gamma t}$, generated by a Γ derived from the molecular dynamics data. Thus, $\bar{\Upsilon}_\alpha$ is the $t \rightarrow 0$ limit of the metastability term. It is not clear if a t -dependent objective function would be appropriate for clustering data that does not arise in a dynamic manner, though this is worth considering.

Another potentially interesting objective function is the determinant of M . It is intriguing because of its simple geometric interpretation: We can show that maximizing $|M|$ is equivalent to maximizing the hypervolume of the $(m-1)$ -simplex formed in the \bar{w}^Δ -representation by *every* subset of m items [55]. This property is attractive since we expect a good clustering to spread the items out in this barycentric representation as much as possible. However, $|M|$ does not have a simple information-theoretic interpretation as does $\Phi(M)$, defined in Eq. (12): $\exp[-\Phi(M)]$ is the product of the fractional cluster certainties, $\bar{\Upsilon}_\alpha$, which are normalized to be unity when the corresponding cluster is completely hard. In contrast,

the value of $|M|$ does not provide a measure of cluster hardness. Moreover, while optimization using either $|M|$ or $\Phi(M)$ tends to minimize overlap, optimization of $|M|$ also tends to equalize the size of the clusters [55], which is not necessarily desirable. Thus, while it is geometrically elegant, this objective function appears to be inferior to $\Phi(M)$.

No one clustering method is likely to be best for all problems, so it is important to match the method to the problem. We expect that MDC will be an advantageous choice in problems that would benefit from its ability to simultaneously determine the number of clusters, provide fuzzy clustering, quantitatively assess the overall certainty of a cluster, and handle irregular cluster shapes. For example, as mentioned in the Introduction, fuzzy assignments might be important in studies of population genetics [2, 3] where they would allow populations to overlap and for migrants to be identified. In the same vein, they would allow detection of overlapping communities in complex networks (e.g., those of the World Wide Web and systems biology) [56]. Fuzzy clustering should also be beneficial in clustering gene expression data: Gene functional redundancy and the multiple roles of proteins are likely to result in overlapping gene clusters, which can not be represented by the hard clusters of traditional methods [57]. Yet another example is fluorescence activated cell sorting (FACS) data: Clusters representing different cell phenotypes often have irregular and fuzzy boundaries [58], so the ability of MDC to cope with these characteristics should be important in softly dissecting the FACS dataspace into cell type-specific regions for cell sorting. These same characteristics may also be useful in automating database curation. For example, Paccanaro et al. [59] have already shown that a spectral clustering method can faithfully reproduce many of the superfamily classifications from a subset of the SCOP protein database [60], and MDC would provide the additional benefits of fuzziness and of indicating the confidence of a particular classification.

Biological data sets pose special difficulties for clustering methods: They are noisy and often contain irrelevant dimensions, which do not help to distinguish clusters. They may, in fact, obfuscate the cluster boundaries, particularly if the items are dispersed in the irrelevant dimensions. For example, genes will have expression levels correlated with only a subset of experimental conditions (e.g., cancer types); moreover, the relevant conditions may vary across genes. However, the diffusive model that underlies MDC suggests that it will be relatively insensitive to this problem: As discussed in Sec. II, MDC identifies clusters as dataspace regions whose *intra*-cluster relaxation times are small compared to their *inter*-cluster relaxation times. By analogy to physical stochastic processes, these time scales are governed by both energetic and entropic factors: “Energetic barriers” are generated by gaps between clusters in the dataspace and (as in transition-state theory) exponentially decrease the inter-cluster transition rates. On the other hand, dispersion

in the irrelevant dimensions increases the “entropic” volume of the cluster, which only increases the intra-cluster relaxation time like the square of the length scale of the dispersion [61]. This behavior probably accounts for the success of MDC in the test problems we have examined that have irrelevant dimensions (e.g., the Parallel problem in Ref. [8] and the Two Diamonds problem in Sec. VB). If necessary, MDC might be improved by combining it with the Clustering on a Subset of Attributes (COSA) method [62], which is designed specifically to address the irrelevant dimension problem. COSA assigns non-uniform relevance to each dimension by manipulating the metric tensor g of Eq. (2) through an iterative search that invokes a clustering procedure at each step. Because of its relative insensitivity to irrelevant dimensions, using MDC for this clustering might increase the convergence rate and improve accuracy within the iterative COSA framework. Incorporating MDC within the COSA framework is now practical given the described, improved efficiency of uncertainty minimization.

Acknowledgments

The authors are grateful to Sally McKee for the use of computational resources and to Vince Weaver for help in administering them. Partial support was provided for B.S.W. by a DOE High-Performance Computer Science Fellowship administered by The Krell Institute, Ames, IA.

APPENDIX A: Γ PRECONDITIONING

Numerical errors can obscure the differences between very small eigenvalues and obfuscate the spectral gap when the range between γ_1 and γ_{N-1} is too large to be faithfully represented numerically. This can occur if clusters are nearly isolated (and hence communicate very slowly) or when two items within a cluster are exceedingly close to another (and hence communicate very rapidly). The former case also occurs when the data contain outliers—items that are distant from the bulk of the items. We avoid these problems by preconditioning Γ . In addition, we improve computational efficiency by sparsifying Γ (i.e., by setting very small transition rates exactly to zero) and by employing efficient sparse matrix algorithms.

To avoid the numerical error problems, we want to precondition Γ so that

$$\gamma_1 \gg \Delta_\gamma, \quad (\text{A1})$$

where Δ_γ is the expected computational error in the eigenvalues. Typically [44, 46]

$$\Delta_\gamma \leq \epsilon \gamma_{N-1},$$

where ϵ is machine precision. To conservatively satisfy Eq. (A1), we want to adjust the very small and/or very

large elements of Γ so that

$$\left(\frac{\gamma_1}{\gamma_{N-1}}\right)^2 \gtrsim \epsilon. \quad (\text{A2})$$

To minimize the effect of this adjustment on the other eigenvalues, this adjustment should yield a γ_1 and γ_{N-1} that are multiplicatively symmetric relative to γ_{mid} , an appropriate midrange frequency. That is, we require

$$\frac{\gamma_{\text{mid}}}{\gamma_1} \sim \frac{\gamma_{N-1}}{\gamma_{\text{mid}}}. \quad (\text{A3})$$

Eqs. (A2) and (A3) will be satisfied if

$$\gamma_1 \gtrsim \gamma_{\text{mid}} \epsilon^{1/4} \quad (\text{A4a})$$

$$\gamma_{N-1} \lesssim \gamma_{\text{mid}} \epsilon^{-1/4}. \quad (\text{A4b})$$

To determine γ_{mid} , we note that $-\Gamma_{i>}$, the magnitude of the largest off-diagonal element in row i of Γ , determines the largest transition rate connecting i to other items. Thus, the median of the $-\Gamma_{i>}$ is a reasonable choice for γ_{mid} . However, to maximize the useful numerical range, if it appears that one, but not the other, of the inequalities in Eqs. (A4) are likely to be satisfied without any adjustment, we shift γ_{mid} . Specifically,

$$\begin{aligned} &\text{If } (\min |\Gamma_{ij}| < \gamma_{\text{mid}} \epsilon^{1/4}) \cap (\max |\Gamma_{ij}| < \gamma_{\text{mid}} \epsilon^{-1/4}) \\ &\quad \text{then } \gamma_{\text{mid}} \leftarrow \max |\Gamma_{ij}| \epsilon^{1/4} \\ &\text{If } (\min |\Gamma_{ij}| > \gamma_{\text{mid}} \epsilon^{1/4}) \cap (\max |\Gamma_{ij}| > \gamma_{\text{mid}} \epsilon^{-1/4}) \\ &\quad \text{then } \gamma_{\text{mid}} \leftarrow \min |\Gamma_{ij}| \epsilon^{-1/4}, \end{aligned}$$

where $|\Gamma_{ij}|$ refers to the magnitudes of the off-diagonal elements.

1. Connected component analysis

To satisfy Eq. (A4a) we perform a standard connected component analysis [63] using threshold

$$\gamma_{\text{lo}} \equiv \gamma_{\text{mid}} \epsilon^{1/4}.$$

This analysis initially assigns items to individual sets and then iteratively merges sets whenever any of their respective members have connecting connectivities $|\Gamma_{ij}| > \gamma_{\text{lo}}$. If distinct sets (i.e., disconnected components) remain at the end, the algorithm creates hard assignment vectors identifying them.

2. High transition rate cutoff

We expect that γ_{N-1} will be of the order of the fastest inter-item transition rate in the system [64]. Thus, we can satisfy Eq. (A4b) by truncating any off-diagonal elements of Γ exceeding

$$\gamma_{\text{hi}} \equiv \gamma_{\text{mid}} \epsilon^{-1/4},$$

i.e., $\Gamma_{ij} \leftarrow -\min(|\Gamma_{ij}|, \gamma_{\text{hi}})$.

3. Sparsification

To reduce memory requirements and improve cache performance, we represent Γ as a sparse matrix by setting very small elements (i.e., $|\Gamma_{ij}| < \gamma_{\text{lo}}/10$) to zero. This improves eigensolver efficiency so that MDC may be practically applied to large problems. For example, for the largest of the scaling benchmarks considered in Section V.B. (i.e., $m = 10$, $N = 20,000$), the sparse Γ matrix held less than 870,000 elements and thus reduced storage by a factor of nearly 500 [65].

4. Diagonal elements

Once the steps above, which modify only the off-diagonal elements of Γ , have been completed, we reset the diagonal elements according to Eq. (9b) so that Eq. (3b) is again satisfied.

APPENDIX B: VARIOUS PROOFS

1. Even distribution of active inequality constraints

We prove here that each cluster must be constrained by exactly $m-1$ inequality constraints at each local minimum of Φ in the feasible region. Consider a local minimum $\vec{M}^{\times \text{free}}$ in the asymmetric M -representation discussed in Sec. III A. Korenblum and Shalloway [8] have already proved that this must be at a vertex of the feasible polytope. The coordinates at the local minimum of the individual free particles, \vec{M}_α^\times ($1 \leq \alpha < m$), satisfy the inequality constraints of Eq. (7a), but their homogeneity means that they will also be satisfied for any $\xi_\alpha \vec{M}_\alpha$ with $\xi_\alpha > 0$. Therefore, the inequality constraints acting on the free particles alone leave the $m-1$ degrees of freedom ξ_α ($1 \leq \alpha < m$) unspecified, and thus they are inadequate to force $\vec{M}^{\times \text{free}}$ to be at a vertex of the feasible polytope. Therefore, at least $m-1$ additional active constraints must come from the inhomogeneous inequality constraints associated with the slave particle [Eq. (16)]. However, the choice of the slave particle [in Eq. (15)] is arbitrary. Therefore, *every* particle must have at least $m-1$ active inequality constraints. But since only $m(m-1)$ inequality constraints are active at a vertex, each of the m particles must have *exactly* $m-1$ inequality constraints active. This proof extends to every vertex of the feasible polytope except for those vertices where at least one of the $\vec{M}_\alpha^\times = 0$ (since multiplying this by ξ_α does not move the particle). This proof does not preclude the possibility that a single item may be associated with multiple active constraints; i.e., it is possible that $w_\alpha(i) = 0$ and $w_\beta(i) = 0$ are both active constraints. {This is the case for the solution to the spiral problem [Figs. 2(c) and (d)] where $w_2(r_1) = 0 = w_3(r_1)$ and also $w_1(r_2) = 0 = w_3(r_2)$.}

2. Invertibility of $\Psi^{\mathcal{R}}$

We prove here that there is at least one subset of m items \mathcal{R} such that $\Psi^{\mathcal{R}}$ is invertible. We define the $m \times N$ matrix Ψ by $\Psi_{ni} \equiv \psi_n(i)$ ($0 \leq n < m; 1 \leq i \leq N$). Since its m rows, i.e., the low-frequency eigenvectors, are linearly independent, Ψ has rank m . Therefore, Ψ also has at least m linearly-independent columns. If the items corresponding to these columns are selected to comprise \mathcal{R} , then the $m \times m$ matrix $\Psi^{\mathcal{R}}$ has full rank and is therefore invertible.

3. Invertibility of M

We prove here that each M corresponding to a local minimum of Φ within the feasible region is invertible: As proved in Appendix B 1, at any such minimum each cluster has $m-1$ active inequality constraints: $m-1$ items lie on each of the m faces of the bounding simplex in the \bar{w}^Δ -representation. Consider a subset of m of these $m(m-1)$ items, \mathcal{R} , which contains one item from each face. It defines an $(m-1)$ -simplex (inscribed within the bounding simplex) with non-zero hypervolume. This hypervolume is proportional to $|W^{\mathcal{R}}|$, implying that $|W^{\mathcal{R}}| \neq 0$ and, with Eq. (20), implying that $|M| \neq 0$. Thus, M is invertible.

This proof only requires an M that places $m-1$ items on each of the m faces of the \bar{w}^Δ -representation bounding simplex; i.e., M is at a vertex of the feasible polytope of the asymmetric M -representation. Therefore, it actually extends to every vertex of the feasible polytope in the asymmetric representation where all the $\bar{M}_\alpha \neq 0$, since we have proven in Appendix B 1 that all the inequality constraints are evenly distributed at such vertices.

4. The bounding simplex in the $\vec{\psi}^\perp$ -representation

Analogously to Eq. (17), we may write

$$W^{\text{vert}} = M \circ \Psi^{\text{vert}},$$

where the columns of Ψ^{vert} are the coordinates of the bounding simplex vertices in the low-frequency eigenvector representation and $W^{\text{vert}} = I$ is the matrix whose rows are the coordinates of the vertices in the \bar{w}^Δ -representation. Inverting this gives $\Psi^{\text{vert}} = M^{-1}$. When $M = M^0$ this and Eq. (22b) imply that $\Psi^{\text{vert}} = \Psi^{\mathcal{R}_c}$, which is consistent with the zeroth-order placement of the representatives at the vertices. When $M = M^*$, the vertices may not correspond to item locations, but, as proved in Appendix B 3, M^* is invertible, so $\Psi^{\text{vert}} = (M^*)^{-1}$. In both cases, the simplex vertex coordinates in the $\vec{\psi}^\perp$ -representation are given by the columns of Ψ^{vert} with the first rows omitted. (Just as for $\Psi^{\mathcal{R}}$, all elements in the first row of Ψ^{vert} are unity for any invertible M [66], in particular, for M^0 and M^* .)

5. Same ordering of item points in the \bar{w}^Δ - and $\vec{\psi}^\perp$ -representations

To simplify the proof of identical ordering, we use the spiral problem illustrated in Fig. 2 as a specific example; the proof is easily generalized. We index the vertices in the \bar{w}^Δ -representation as discussed in Sec. III B 1. For example, the top vertex in panel (c) is vertex 3 and we denote this as point v_3 . We carry the same labeling over to the $\vec{\psi}^\perp$ -representation.

Determining the item ordering relative to the bounding simplex faces is easy in the \bar{w}^Δ -representation: Because this provides barycentric coordinates, the distance of a point i from the side opposite to vertex α is just $w_\alpha(i)$, with the sign negative if the point lies outside the simplex. Thus, the ordering is determined simply by comparing these distances. We relate this ordering to the ordering in the $\vec{\psi}^\perp$ -representation in a few steps. First, note that the distance of point i from the side opposite v_2 is linearly related to the area of the triangle having vertices at points i , v_1 , and v_3 , with sign depending on triangle orientation. This signed area is proportional to the ratio of determinants

$$A = \frac{|\bar{w}(i) \otimes \hat{e}_1 \otimes \hat{e}_3|}{|\hat{e}_2 \otimes \hat{e}_1 \otimes \hat{e}_3|},$$

where $\bar{w}(i) \otimes \hat{e}_1 \otimes \hat{e}_3$ is the 3×3 matrix formed by stacking the three row vectors and the denominator (which will always be ± 1) is inserted to adjust the sign. Second, note that since

$$\begin{aligned} \bar{w}(i) \otimes \hat{e}_1 \otimes \hat{e}_3 &= M \circ [\vec{\psi}(i) \otimes \vec{\psi}_{v_1} \otimes \vec{\psi}_{v_3}] \\ \hat{e}_2 \otimes \hat{e}_1 \otimes \hat{e}_3 &= M \circ [\vec{\psi}_{v_2} \otimes \vec{\psi}_{v_1} \otimes \vec{\psi}_{v_3}], \end{aligned}$$

where $\vec{\psi}_{v_k}$ is the m -vector having the coordinates of vertex v_k in the low-frequency eigenvector space, we have

$$A = \frac{|\vec{\psi}(i) \otimes \vec{\psi}_{v_1} \otimes \vec{\psi}_{v_3}|}{|\vec{\psi}_{v_2} \otimes \vec{\psi}_{v_1} \otimes \vec{\psi}_{v_3}|}. \quad (\text{B1})$$

Third, since all the vectors in Eq. (B1) have $\psi_0(i) = 1$ ($\forall i$), A is proportional to the signed area of the triangle having vertices i , v_1 , and v_3 in the $\vec{\psi}^\perp$ -representation, which will be positive if i is within the triangle and negative if it is outside the triangle. Fourth, this area is proportional to the distance of point i from the side opposite to v_2 in the $\vec{\psi}^\perp$ -representation. Combining all these proportionalities proves that the distance of point i from the side opposing a vertex in the \bar{w}^Δ -representation is proportional to the distance in the $\vec{\psi}^\perp$ -representation.

APPENDIX C: GREEDY ALGORITHM FOR SELECTING \mathcal{R}

The goal of the algorithm is to choose the subset of items \mathcal{R} that approximately defines the $(m-1)$ -

simplex having maximum hypervolume V_{m-1} in the $\vec{\psi}^\perp$ -representation. If the hypervolume, V_{m-2} , of one face of the simplex is already determined, V_{m-1} is proportional to the distance of the excluded vertex from that face. [For example, in the case of a 2-simplex (a triangle), this is the familiar area = 1/2 base \times height rule, where “base” is the length of the determined simplex face and “height” is the distance of the other point from that face.] This suggests a natural greedy algorithm: (a) initialize by finding the $(q-1=1)$ -simplex of greatest length, (b) extend the $(q-1)$ -simplex to a q -simplex by finding the item that is furthest from the hypersurface that embeds the $(q-1)$ -simplex, (c) $q \leftarrow q+1$ and return to step (b) until $q = m$.

Specifically,

1. Initialize:

Select the two items i_1 and i_2 that maximize $\|\vec{\psi}^\perp(i_2) - \vec{\psi}^\perp(i_1)\|$.
 $\mathcal{R} = \{i_1, i_2\}$.
 $q = 2$.

2. Repeat while $q < m$:

(a) Select the item i_{q+1} that maximizes

$$d^\perp(i_{q+1}) = \|\mathcal{P}^q \odot [\vec{\psi}^\perp(i_{q+1}) - \vec{\psi}^\perp(i_1)]\|,$$

where

$$\mathcal{P}_{nn'}^q = I_{nn'} -$$

$$\sum_{q'=2}^q \frac{[\vec{\psi}^\perp(i_{q'}) - \vec{\psi}^\perp(i_1)]_n [\vec{\psi}^\perp(i_{q'}) - \vec{\psi}^\perp(i_1)]_{n'}}{\|\vec{\psi}^\perp(i_{q'}) - \vec{\psi}^\perp(i_1)\|^2}.$$

(b) $\mathcal{R} \leftarrow \mathcal{R} \cup i_{q+1}$

(c) $q \leftarrow q+1$

Here \odot denotes the inner product within the $(m-1)$ -dimensional $\vec{\psi}^\perp$ space and \mathcal{P}^q is the projection matrix in this space that removes the components of $[\vec{\psi}^\perp(i_{q+1}) - \vec{\psi}^\perp(i_1)]$ that lie within the subspace containing the $(q-1)$ -simplex. Therefore, $d^\perp(i_{q+1})$ is the distance of $\vec{\psi}^\perp(i_{q+1})$ from the subspace, and the q -simplex formed by adding $\vec{\psi}^\perp(i_{q+1})$ as a vertex is that of maximum hypervolume containing the previously computed $(q-1)$ -simplex as one of its faces.

-
- [1] R. J. Cho, M. J. Campbell, E. A. Winzeler, L. Steinmetz, A. Conway, L. Wodicka, T. G. Wolfsberg, A. E. Gabriellian, D. Landsman, D. J. Lockhart, et al., *Molecular Cell* **2**, 65 (1998).
 - [2] J. K. Pritchard, M. Stephens, and P. Donnelly, *Genetics* **155**, 945 (2000).
 - [3] N. Patterson, A. L. Price, and D. Reich, *PLoS Genet.* **2**, 2074 (2006).
 - [4] B. S. Everitt, S. Landau, and M. Leese, *Cluster Analysis* (Arnold, London, 2001).
 - [5] J. Shi and J. Malik, in *Proceedings of IEEE Conference on Computer Vision and Pattern Recognition* (1997), pp. 731–737.
 - [6] S. D. Kamvar, D. Klein, and C. D. Manning, in *Proc. International Joint Conference on Artificial Intelligence* (2003).
 - [7] A. Y. Ng, M. I. Jordan, and Y. Weiss, in *Proceedings of the 14th Neural Information Processing Systems Conference* (2002).
 - [8] D. Korenblum and D. Shalloway, *Phys. Rev. E* **67**, 056704 (2003).
 - [9] Spectral graph theory methods sometimes analyze the *normalized Laplacian* $\mathcal{L} \equiv D_S^{-\frac{1}{2}} \Gamma D_S^{-\frac{1}{2}}$. Related methods analyze the Markov matrix $T \equiv D_S^{-\frac{1}{2}} S D_S^{-\frac{1}{2}} = I - \mathcal{L}$, where I is the identity matrix.
 - [10] ψ_0 may be chosen to satisfy Eq. (4b) even in a degenerate system having multiple zero eigenvalues.
 - [11] An exception is Ref. [67], which uses more than m eigenvectors in the projected representation.
 - [12] D. A. Spielman and S.-H. Teng, in *Proc. Annual Symposium on Foundations of Computer Science* (IEEE Computer Society, Washington, DC, 1996), pp. 96–105.
 - [13] S. T. Barnard and H. D. Simon, *Concurrency: Practice and Experience* **6**, 101 (1994).
 - [14] P. K. Chan, M. D. F. Schlag, and J. Y. Zien, in *ACM IEEE Design Automation Conference* (ACM Press, New York, NY, 1993), pp. 749–754.
 - [15] H. D. Simon and S.-H. Teng, *SIAM J. Scientific Computing* **18**, 1436 (1997).
 - [16] D. Verma and M. Meilă, Tech. Rep. UW CSE 03-05-01, University of Washington (2003).
 - [17] M. Meilă and J. Shi, in *Proc. International Workshop on Artificial Intelligence and Statistics* (2001).
 - [18] L. Zelnik-Manor and P. Perona, in *Proc. Neural Information Processing Systems Conference* (2004).
 - [19] H. S. Chan and K. A. Dill, *Phys. Today* **46**, 24 (1993).
 - [20] D. Shalloway, *J. Chem. Phys.* **105**, 9986 (1996).
 - [21] M. B. Eisen, P. T. Spellman, P. O. Brown, and D. Botstein, *Proc. Natl. Acad. Sci. USA* **95**, 14863 (1998).
 - [22] M. Weber, Tech. Rep. 03-04, Konrad-Zuse-Zentrum für Informationstechnik Berlin (2003).
 - [23] M. Weber, W. Rungtarityotin, and A. Schliep, Tech. Rep. 04-39, Konrad-Zuse-Zentrum für Informationstechnik Berlin (2004).
 - [24] G. W. Stewart, in *Mathematical Computer Performance and Reliability*, edited by G. Iazeolla, P. J. Courtois, and A. Hordijk (Elsevier, North Holland, 1984), pp. 287–302.
 - [25] Without loss of generality, the diffusion coefficient, which would normally appear in Eq. (9a), is set to unity.
 - [26] M. Belkin and P. Niyogi, *Neural Computation* **15**, 1373 (2003).
 - [27] D. Harel and Y. Koren, in *Proc. Conference on Foundations of Software Technology and Theoretical Computer Science* (Springer-Verlag, London, UK, 2001), pp. 18–41.
 - [28] B. Nadler, S. Lafon, R. R. Coifman, and I. G. Kevrekidis, *Applied and Computational Harmonic Analysis* **21**, 113 (2006).
 - [29] L. Yen, D. Vanvyve, F. Wouters, F. Fouss, M. Verleyen, and M. Saerens, in *Proc. European Symposium on*

- Artificial Neural Networks* (2005), pp. 317–324.
- [30] G. L. Scott and H. C. Longuet-Higgins, in *Proceedings of British Machine Vision Conference* (1990), pp. 103–108.
- [31] For $m > 2$, the slave inequality constraint boundaries do not intersect at a point but in the subspace where Eq. (16) is an equality for all items. This condition can be expressed as $\sum_{k=1}^{m(m-1)} Z_{ik} M_k^{\text{free}} = 1$ ($\forall i$), where $M_k^{\text{free}} \equiv M_{\alpha n}$ with $\alpha \equiv 1 + \left\lfloor \frac{k-1}{m} \right\rfloor$, $n \equiv (k-1) \bmod m$, and $Z_{ik} \equiv \psi_{k'}(i)$ with $k' \equiv (k-1) \bmod m$. (M_k^{free} is the flattened form of the supervector \vec{M}_k^{free} .) Z_{ik} has m independent columns, i.e., it contains $m-1$ copies of each of the m low-frequency ψ_n . Therefore, its rank is m and it only imposes m restrictions on the $m(m-1)$ variables. Thus, the intersection of the inhomogeneous constraints occurs in a subspace of dimension $m(m-1) - m = m(m-2)$.
- [32] Eq. (21) breaks the permutation symmetry by assigning each representative to a specific cluster index.
- [33] To prove this, we post-multiply Eq. (22b) by $\Psi^{\mathcal{R}_c}$ and sum to get $1 = \sum_{\alpha} I_{\alpha\beta} = \sum_{\alpha n} M_{\alpha n}^0 \Psi_{n\beta}^{\mathcal{R}_c}$ ($\forall \beta$). Since $\Psi_{0\beta}^{\mathcal{R}} \equiv \psi_0(r_\beta) = 1$ ($\forall \beta$), this is solved by $\sum_{\alpha} M_{\alpha n}^0 = \delta_{n0}$. Moreover, since $\Psi^{\mathcal{R}}$ is invertible, this solution is unique, thereby proving Eq. (23).
- [34] Although they are constructed from the same components, do not confuse the m N -vectors \mathbf{w}_α^* , which are vectors over the space of items, with the N m -vectors $\vec{w}^*(i)$, which are vectors over the space of clusters. (These vectors can be viewed as the rows and columns, respectively, of an $m \times N$ matrix W^* .)
- [35] H. S. M. Coxeter, *Introduction to Geometry* (John Wiley & Sons, 1969), 2nd ed.
- [36] Since the covariance matrix, $C_{mn} \equiv \psi_m \cdot \psi_n = \delta_{mn}$, is diagonal, the item points in the $\vec{\psi}^\perp$ -representation have principal components ψ_n ($0 < n < m$) and center of mass at the origin.
- [37] We ignore the rare case where LP may have multiple solutions.
- [38] Interior point methods have complexity $O(m^3 N_c^{1.5} L / \log N_c)$, where $L = \Omega(\log(N_c))$ [68]. Simplex methods require $O(\min(N_c^2, m^4))$ pivot steps [69]. The complexity of each pivot step is $O(N_c^2)$, as that is the size of matrix that is updated. Thus, the number of operations for simplex methods, like that of interior point methods, grows at least as fast as $N_c^{1.5}$.
- [39] In the spiral problem the representatives at vertices 1 and 2 each contribute two active constraints to the solution M^* . Because the left side pivots out during refinement, the representative at vertex 3 only contributes one of two constraints active at M^0 ; the second constraint associated with this vertex comes from the item identified by the arrow in Fig. 2(f). Specifically, the constraints active at M^* are $w_\alpha(i) = 0$ where $(\alpha, i) = (2, r_1), (3, r_1), (1, r_2), (3, r_2), (1, r_3)$, and $(2, x_3)$, where x_3 is the index of the item identified by the arrow. In this problem, the algorithm identifies all these in a single step.
- [40] This number is somewhat arbitrary and is chosen to limit computational cost on the assumption that the number of potential clusters to be identified at a single level of recursion is < 20 . A larger value could be used if needed.
- [41] R. Lehoucq and D. Sorensen, in *Templates for the Solution of Algebraic Eigenvalue Problems: A Practical Guide*, edited by Z. Bai, J. Demmel, J. Dongarra, A. Ruhe, and H. van der Vorst (SIAM, Philadelphia, 2000).
- [42] G. H. Golub and C. F. Van Loan, *Matrix Computations* (John Hopkins U. Press, Baltimore, Md., 1996), chap. 9, 3rd ed.
- [43] A. Ultsch, in *Workshop on Self-Organizing Maps* (Paris, 2005), pp. 75–82.
- [44] E. Anderson, Z. Bai, S. Blackford, J. Demmel, J. Dongarra, J. Du Croz, A. Greenbaum, S. Hammarling, A. McKenney, and D. Sorensen, *LAPACK Users' Guide* (SIAM, Philadelphia, PA, 1999).
- [45] C. Stimming, *Lapack++* <http://lapackpp.sourceforge.net> (2008).
- [46] R. B. Lehoucq, D. C. Sorensen, and C. Yang, *ARPACK Users' Guide: Solution of Large-Scale Eigenvalue Problems with Implicitly Restarted Arnoldi Methods* (SIAM, Philadelphia, 1998).
- [47] F. A. M. Gomes and D. C. Sorensen, Tech. Rep. TR97729, Rice University (1997).
- [48] A. Makhorin, *GNU linear programming kit: Reference manual* <http://www.gnu.org/software/glpk> (2006).
- [49] Actually, Ref. [23] uses a slightly different variant in which the greedy algorithm is initialized by selecting the item that is farthest from the origin rather than the two items that are farthest from each other. We suspect this makes little difference in practice.
- [50] P. Deuffhard, W. Huisinga, A. Fischer, and C. Schütte, *Lin. Alg. Appl.* **315**, 39 (2000).
- [51] C. Schütte and W. Huisinga, *Handbook of Numerical Analysis* **X**, 699 (2003).
- [52] P. Deuffhard and M. Weber, *Lin. Alg. Appl.* **398**, 161 (2005).
- [53] S. Kube and M. Weber, *J. Chem. Phys.* **126**, 024103 (2007).
- [54] F. Noé, I. Horenko, C. Schütte, and J. Smith, *J. Chem. Phys.* **126**, 155102 (2007).
- [55] The hypervolume in the \vec{w}^Δ -representation of the $(m-1)$ -simplex formed by any subset \mathcal{R} of m items (not necessarily representatives) is proportional to $|W^{\mathcal{R}}|$, which, according to Eq. (17), is $|W^{\mathcal{R}}| = |M| |\Psi^{\mathcal{R}}|$. Thus, the hypervolume for every subset is proportional to $|M|$, although the constant of proportionality, $|\Psi^{\mathcal{R}}|$, is different in each case. Therefore, maximizing $|M|$ maximizes the hypervolume of each $(m-1)$ -simplex. Moreover, as discussed in Appendix B 4, $\Psi^{\text{vert}} = M^{-1}$, and since $|\Psi^{\text{vert}}|$ is proportional to the area of the inequality constraint boundary $(m-1)$ -simplex in the $\vec{\psi}^\perp$ -representation, maximizing $|M|$ minimizes the hypervolume of this simplex. To see that maximizing $|M|$ tends to equalize the cluster sizes, note that $|M| = |M \circ M^T|^{1/2} = |\Omega|^{1/2}$, where $\Omega_{\alpha\beta} \equiv \mathbf{w}_\alpha \cdot \mathbf{w}_\beta$. [The equivalence follows from Eq. (6) and the orthonormality of the eigenvectors.] The off-diagonal elements of Ω are the cluster overlaps and will be small compared to the diagonal elements. Therefore the determinant is dominated by the product of the diagonal elements, $\prod_{\alpha} \mathbf{w}_\alpha \cdot \mathbf{w}_\alpha \equiv \prod_{\alpha} (1 - \sum_{\beta \neq \alpha} \mathbf{w}_\beta) \approx \prod_{\alpha} 1 \cdot \mathbf{w}_\alpha$. This will be maximized when all the $1 \cdot \mathbf{w}_\alpha$ (i.e., the fractions of items assigned to each cluster) are equal.
- [56] J. Reichardt and S. Bornholdt, *Phys. Rev. Lett.* **93**, 218701 (2004).
- [57] A. P. Gasch and M. B. Eisen, *Genome Biol.* **3**, 1 (2002).
- [58] D. Jeffries, I. Zaidi, B. de Jong, M. J. Holland, and D. J. C. Miles, *Cytometry Part A* **73A**, 857 (2008).

- [59] A. Paccanaro, J. A. Casbon, and M. A. S. Saki, Nucl. Acids Res. **34**, 1571 (2006).
- [60] A. G. Murzin, S. E. Brenner, T. Hubbard, and C. Chothia, J. Mol. Biol. **247**, 536 (1995).
- [61] To see this, consider the characteristic relaxation time of a diffusive harmonic oscillator as a function of its fluctuation length.
- [62] J. H. Friedman and J. J. Meulman, J. R. Statist. Soc. B **66**, 1 (2004).
- [63] T. H. Cormen, C. E. Leiserson, R. L. Rivest, and C. Stein, *Introduction to Algorithms* (MIT Press, Cambridge, MA, 2001), chap. 22.3.
- [64] Inter-item transition rates can combine to generate eigenvalues that are higher than the individual rates. But, since we expect that each item will communicate rapidly only with a relatively small number of near neighbors (even for large N), we don't expect γ_{N-1} to exceed $\max |\Gamma_{ij}|$ by a factor that is significant on the scale of $\epsilon^{-1/4}$. This effect can be ignored.
- [65] In computational practice, we sparsify Γ based on the values of the corresponding distances d_{ij} before the Γ_{ij} are computed from Eq. (9a). This saves unnecessary exponentiations for the large fraction of elements of Γ_{ij} that will be set to zero anyway. For this purpose, we set $\Gamma_{ij} \leftarrow 0$ whenever $d_{ij} > d_{\max}$, where d_{\max} is calculated by numerically inverting Eq. (9a) with $\Gamma_{ij} = -\gamma_{\text{lo}}/10$. In this procedure, γ_{mid} , which is needed to compute γ_{lo} , is computed by substituting $d_{ij} = \text{median} \{d_{i<} : 1 \leq i \leq N\}$ into Eq. (9a).
- [66] To prove this, multiply both sides of Eq. (19) by $M_{n\beta}^{-1}$ and sum over $n = 0, \dots, m-1$. This gives $1 = M_{0\beta}^{-1}$.
- [67] C. J. Alpert, A. B. Kahng, and S.-Z. Yao, Discrete Applied Mathematics **90**, 3 (1999).
- [68] K. M. Anstreicher, SIAM J. Optim. **9**, 803 (1999).
- [69] I. Adler, R. M. Karp, and R. Shamir, J. Complexity **3**, 372 (1987).